A sound idea: Manipulating domain walls in magnetic nanowires using surface acoustic waves

J. Dean,[1] M. T. Bryan,[2] J. D. Cooper,[3] A. Virbule,[1] J. E. Cunningham,[3] and T. J. Hayward[1]
[1]*Department of Materials Science and Engineering, University of Sheffield, Sheffield S1 3JD, United Kingdom*
[2]*Department of Cardiovascular Science, University of Sheffield, Sheffield S10 2RX, United Kingdom*
[3]*School of Electronic and Electrical Engineering, University of Leeds, Leeds LS2 9JT, United Kingdom*

(Received 17 June 2015; accepted 18 September 2015; published online 8 October 2015)

We propose a method of pinning and propagating domain walls in artificial multiferroic nanowires using electrically induced surface acoustic waves. Using finite-element micromagnetic simulations and 1D semi-analytical modelling, we demonstrate how a pair of interdigitated acoustic transducers can remotely induce an array of attractive domain wall pinning sites by forming a standing stress/strain wave along a nanowire's length. Shifts in the frequencies of the surface acoustic waves allow multiple domain walls to be synchronously transported at speeds up to 50 ms^{-1}. Our study lays the foundation for energy-efficient domain wall devices that exploit the low propagation losses of surface acoustic waves to precisely manipulate large numbers of data bits. © *2015 AIP Publishing LLC*.
[http://dx.doi.org/10.1063/1.4932057]

Domain walls (DWs) in magnetic nanowires[1] have great technological potential through the development of "racetrack" memory devices.[2] In these devices, DWs separate magnetically bi-stable domains, the orientations of which represent binary data. Synchronously moving the DWs transports data along the nanowires, thus facilitating read/write operations.

A major challenge in the development of racetrack memory has been finding efficient methods of transporting DWs. Although DWs in soft-ferromagnetic nanowires can be propagated at modest applied fields ~10 Oe,[3] neighbouring DWs travel in opposite directions, making synchronous data transport impossible unless complex "ratcheted" nanowires[4,5] or field pulses with intricate spatial[6] or temporal profiles[7] are employed. Moving DWs via spin-torque effects is a more attractive approach, since neighbouring DWs travel uni-directionally. However, current-induced DW transport is inefficient and unreliable in soft ferromagnetic systems,[8,9] with complex multilayer nanowires exploiting spin-orbit effects[10–12] or containing antiferromagnetically coupled layers[13] being required to obtain fast and reliable DW motion at typical experimental current densities.

Previously, we have shown that artificial multiferroic systems, where magnetostrictive nanowires are coupled to electrically contacted piezoelectric layers, offer alternative routes to obtaining synchronous DW motion.[14] In this approach, electrically induced strains in the piezoelectric layer produce local variations in the nanowire's magnetic anisotropy by the Villari effect. These can then be utilized to both pin and synchronously propagate DWs. The approach is attractive because it is voltage rather current driven, and thus is expected to be power efficient. Furthermore, in contrast to both field- and current-induced approaches, where interactions are impulse-based, in the multiferroic approach DWs are constantly confined within a stress-induced potential well, offering precise control of the DWs' positioning. However, the necessity of fabricating arrays of electrical contacts makes for complex device designs when compared to the simple, two-terminal configurations required for current-induced motion.

In this letter, we use finite-element micromagnetic simulations to propose an alternative method of pinning and propagating DWs in artificial multiferroic systems. In this approach, two counter-propagating surface acoustic waves (SAWs) are launched into a piezoelectric substrate using a pair of interdigitated transducers (IDTs), thus forming a standing stress/strain wave (SW) along magnetic nanowires placed between them. We have used such standing SAWs previously both to control the position of particles in overlaid microfluidic systems[15] and to modify single-electron transport in GaAs/AlGaAs channels.[16] SWs have also been used previously to manipulate the switching and dynamics of continuous ferromagnetic films.[17–20] Here, we show that a SW creates arrays of DW pinning sites within the nanowires and go on to explain these interactions using a semi-analytical 1D model.[21] We then demonstrate how applying small shifts to the frequency of the transducers allows multiple DWs to be synchronously transported through the nanowires at velocities up to 50 ms^{-1}. Our results indicate the feasibility of multiferroic technologies where electrically induced acoustic waves are used to remotely manipulate DWs.

A schematic of the simulated system is presented in Fig. 1. A $Fe_{70}Ga_{18}B_{12}$ nanowire, with width, $w = 100$ nm, thickness, $t = 2$ nm, and length, $l = 2\,\mu$m, is coupled to a piezoelectric lead zirconate titanate (PZT) substrate between a pair of IDTs. The IDTs have finger spacing $s_{IDT} = 125$ nm and thus produce SAWs with wavelength $\lambda = 500$ nm at resonance. We chose form the nanowire from $Fe_{70}Ga_{18}B_{12}$ as it has soft magnetic properties, similar to Permalloy, while also having a high saturation magnetostriction, $\lambda_s = 70$ ppm.[22] A low film thickness was selected because preliminary data suggested that this enhanced useful SAW-DW interactions.

We assumed that the SAWs took the form of pure Rayleigh waves. Neglecting piezoelectric corrections and solving the Rayleigh equation[23] for a material with the elastic proprieties of isotropic PZT (Young's modulus

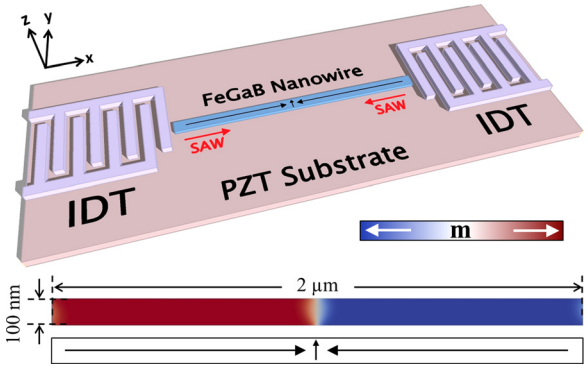

FIG. 1. Schematic diagram of the proposed device. Domain walls in a $Fe_{70}Ga_{18}B_{12}$ nanowire are controlled using counter-propagating surface acoustic waves injected into a lead zirconate titanate (PZT) substrate by a pair of interdigitated transducers (IDTs). The lower figure shows the initial magnetisation configuration of the nanowire as simulated using finite-element micromagnetics.

$E_{PZT} = 100\,GPa$ and Poisson's ratio $\nu_{PZT} = 0.3$ (Ref. 14)), we obtained a SAW velocity of $v_{SAW} = 2114\,ms^{-1}$, and thus an IDT resonance frequency, $f_{IDT} = 4.23\,GHz$. Assuming perfect strain coupling between the substrate and the nanowire (elastic properties: $E_{FeGaB} = 100\,GPa$, $\nu_{FeGaB} = 0.3$ (Ref. 14)), we followed Ref. 23 to obtain the forms of the counter-propagating stress waves generated in the magnetic layer

$$\begin{pmatrix} \sigma_{xx} \\ \sigma_{yy} \\ \sigma_{zz} \\ \sigma_{xy} \\ \sigma_{zx} \\ \sigma_{yz} \end{pmatrix} = A_{SAW} \begin{pmatrix} \sin(kx \mp \omega t) \\ 0 \\ -\sin(kx \mp \omega t) \\ 0 \\ \frac{3}{8}\sin\left(kx \mp \omega t \pm \frac{\pi}{2}\right) \\ 0 \end{pmatrix}, \qquad (1)$$

where A_{SAW} is the amplitude of the stress wave, as determined by the strength of the excitation to the IDTs. $k = \frac{2\pi}{\lambda}$ and $\omega = 2\pi f_{IDT}$. Physically, Eq. (1) represents a "rolling" motion of the substrate's surface, with each point on it tracing an elliptical orbit in the x-z plane.[23] We note that the small ratio of nanowire thickness to λ allows us to neglect the exponential decay of the SAW amplitude with depth.

We modelled the magnetisation dynamics of the nanowire by adapting an in-house finite element micromagnetic code previously used to model static stress effects in magnetic materials[24] to include the influence of time-dependent stresses. The magnetic properties of $Fe_{70}Ga_{18}B_{12}$ were extracted from Ref. 22: saturation magnetisation, $M_s = 1074\,kA\,m^{-1}$, exchange stiffness, $A = 13\,pJ\,m^{-1}$, damping constant, $\alpha = 0.02$, magnetocrystalline anisotropy constant, $K = 0$, and saturation magnetostriction, $\lambda_s = 70\,ppm$. The system was initialised in the head-to-head transverse DW configuration[25] shown in Fig. 1.

In Fig. 2(a), we illustrate how DWs responded to the introduction of a SW formed by counter-propagating SAWs with $A_{SAW} = 30\,MPa$. In each of the simulations presented, the central antinode of the standing wave was displaced from the DW's initial location by a distance $\Delta d = -250\,nm$ to 250 nm. The data show that the DWs moved rapidly to the nearest antinode of the SW, following an oscillating

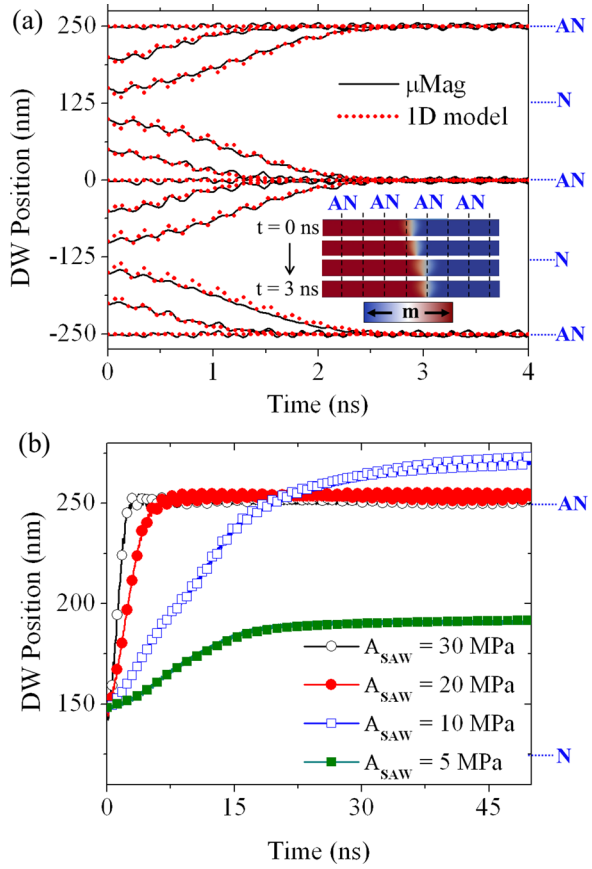

FIG. 2. (a) Results of micromagnetic simulations showing how the position of a domain wall evolves when it is placed at variable distances from the central antinode of a standing stress/strain wave ($A_{SAW} = 30\,MPa$, $\lambda = 500\,nm$, and $f_{IDT} = 4.23\,GHz$). The dotted lines indicate the results of equivalent simulations performed using a 1D semi-analytical model. The inset shows the dynamics of a domain wall initially located 150 nm from the standing wave's central antinode ($\Delta d = -150\,nm$). (b) Variation of localisation behaviour with SAW amplitude for $\Delta d = -150\,nm$. Open circles: $A_{saw} = 30\,MPa$. Closed circles: $A_{saw} = 20\,MPa$. Open squares: $A_{SAW} = 10\,MPa$. Closed squares: $A_{SAW} = 5\,MPa$.

trajectory that reflected the oscillation of the driving stresses. This is further illustrated in the inset to Fig. 2(a) which shows DW dynamics for $\Delta d = -150\,nm$. Here, the DW traversed the 100 nm distance to the nearest antinode in ~2 ns, suggesting a net drift velocity $\sim 50\,ms^{-1}$. Fig. 2(b) shows how the dynamics of the DW were modified as A_{SAW} was reduced. Both the speed and strength of the localisation decreased as A_{SAW} became smaller, with significant localisation only occurring for $A_{SAW} \geq 10\,MPa$. At this lower value of A_{SAW}, the DW drift velocity had reduced to $\sim 5\,ms^{-1}$, and the oscillating character of its motion during its linear drift was more clearly visible.

The data presented in Fig. 2 indicate the enticing possibility of remotely generate arrays of attractive, switchable pinning potentials using SAWs. However, this result is somewhat surprising, as when DWs are manipulated using static stresses,[14] they become pinned at regions of maximum compressive stress. In contrast, the antinodes of the SWs represent regions that alternate dynamically between compressive *and* tensile stress.

To gain a physical understanding of the interaction between the DWs and the SAWs, we utilised the 1D semi-analytical model developed in Ref. 21. In the model, the

instantaneous state of the DW is defined by two parameters, q, its x-axis position and φ, the angle the DW's transverse magnetisation makes with the z-axis. In the absence of magnetic fields, the DWs dynamics can then be modelled by solving

$$\dot{q} = \frac{\Delta}{2(1+\alpha^2)}(-\gamma_0 M_S(N_z - N_y)\sin 2\varphi - f + \alpha g), \quad (2)$$

$$\dot{\varphi} = \frac{1}{2(1+\alpha^2)}(\alpha\gamma_0 M_S(N_z - N_y)\sin 2\varphi + \alpha f + g), \quad (3)$$

where the dots denote a time derivative, γ_0 is the gyromagnetic ratio = 221 kHz/(A/m), and $N_{z,y}$ are the nanowire's demagnetising factors.[26] Δ is the DW width parameter and is a function of both φ and the local stress at the DW location.[21] The stresses produced by the SAWs enter the DW dynamics through terms f and g. Neglecting inactive stress components, we have

$$f = \frac{3\gamma_0\lambda_S}{\mu_0 M_S}[\pi\Delta\sigma'_{xz}\sin\varphi - \sigma_{zz}\sin 2\varphi], \quad (4)$$

$$g = \frac{-3\gamma_0\lambda_S}{2\mu_0 M_S}\pi\Delta\sigma'_{xx}, \quad (5)$$

where μ_0 is the permeability of free space, and σ'_{ij} represents $\frac{d\sigma_{ij}}{dx}$.

Fig. 2(a) compares the results of micromagnetic simulations and the predictions of the semi-analytical model for $A_{SAW} = 30$ MPa. Excellent agreement between the two models was achieved once Δ was multiplied by 1.5, corresponding to an increase in Δ from 28.5 nm to 42.8 nm in the absence of applied stresses. We note that the revised value was close to the (width-averaged) value of $\Delta = 38.8$ nm derived from the simulated DW configuration. Similar increases of DW widths have been required to obtain agreement between the results of 1D models and micromagnetic simulations in previous studies.[21]

Having demonstrated the ability of the 1D model to reproduce the simulated DW dynamics, we used it to reveal the physical mechanisms underlying DW motion. Eq. (2) contains three terms that contribute to DW motion. The first term $(-\gamma_0 M_S(N_z - N_y)\sin 2\varphi)$ represents the influence of the demagnetizing field created by changes in φ. The second term $(-f)$ contains stress components σ'_{xz} and σ_{zz}, while the third term (αg) contains σ'_{xx} alone. The contributions of these three terms to $\dot{q}$ are plotted for $\Delta d = -150$ nm in Fig. 3(a). Fig. 3(b) presents a numerical integration of the data in Fig. 3(a), allowing terms that cause displacement to be differentiated from those that cause oscillation alone.

The data show that the DW's demagnetizing field makes the largest contribution to $\dot{q}$. Thus, we deduce that the primary role of the SW is to drive oscillations of φ, rather than to displace DWs directly. Plotting the three terms in Eq. (3) allows us to deduce which stress components have the strongest influence on $\dot{\varphi}$, and thus dictate the overall dynamics of the system. Fig. 3(c) presents this analysis and shows g to be the dominant factor. The active term is thus σ'_{xx}, the gradient of stress along the nanowires length. The dominance of this term is further demonstrated in Fig. 3(d), which compares simulations performed using σ_{xx} alone with those incorporating all three components of the Rayleigh wave. Only small differences can be observed between the simulations, with DWs localising slightly faster in the simulations where all stress terms were active, indicating that σ_{zz} and σ'_{xz} played minor roles in the DWs' dynamics.

The above analysis allows a physical understanding of why DWs are attracted to the antinodes of a SW. The SW drives oscillations in φ, which in turn drives oscillations in q through the demagnetising field. The oscillations in q lag $\sim \pi/2$ behind those in φ (note that $\dot{q} \propto \varphi$ in (2)), and thus DWs appear to carry "momentum" that continues to carry them forward until φ passes through the plane of the nanowire, reversing the direction of their motion. σ'_{xx} is maximised at the nodal points, so if a DW travels towards an antinode during the first half of an oscillation cycle, it will experience smaller driving forces in the second half and vice-versa, thus producing a net displacement. Therefore, the DWs undergo a ratcheted, oscillating motion towards the antinode points, where the driving interaction is minimised

We note that, for the nanowire we simulated, DW localisation was relatively weak, with the DWs becoming depinned from the SW antinodes once $H_x > 2.5 \pm 0.5$ Oe

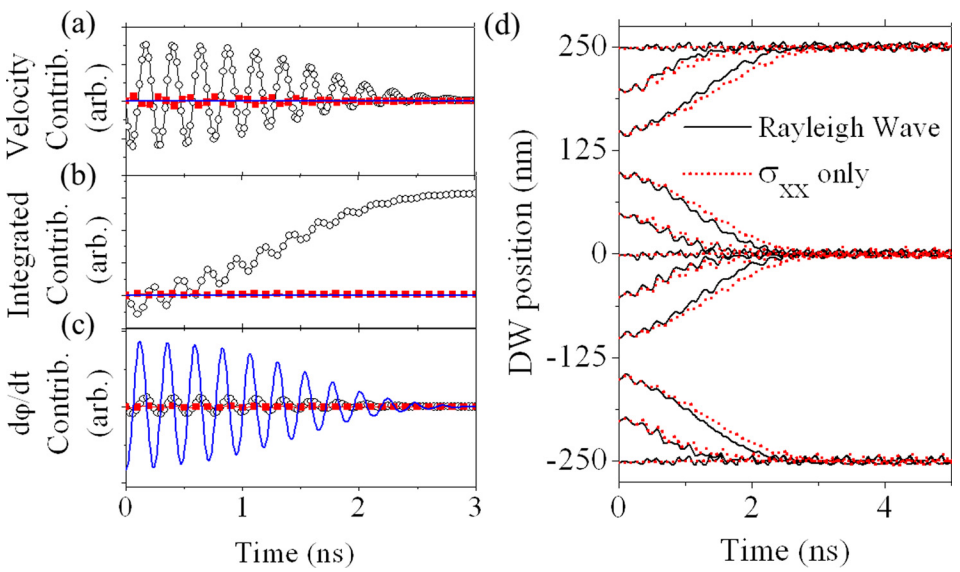

FIG. 3. Analysis of DW motion for $\Delta d = -150$ nm using a 1D semi-analytical model. (a) Contributions of the three terms in Eq. (2) to $\dot{q}$. Open circles: $-\gamma_0 M_S(N_z - N_y)\sin 2\varphi$. Closed squares: f. No symbols: αg. (b) Shows a time integration of (a). (c) Contributions of the three terms in Eq. (3) to $\dot{\varphi}$. Open circles: $\alpha M_S(N_z - N_y)\sin 2\varphi$. Closed squares: αf. No symbols: g. (d) Comparison of the results of micromagnetic simulations using the full stress profile of a Rayleigh wave (unbroken lines) with those incorporating σ_{xx} only (dotted lines). For all of simulations, $A_{SAW} = 30$ MPa, $\lambda = 500$ nm, and $f_{IDT} = 4.23$ GHz.

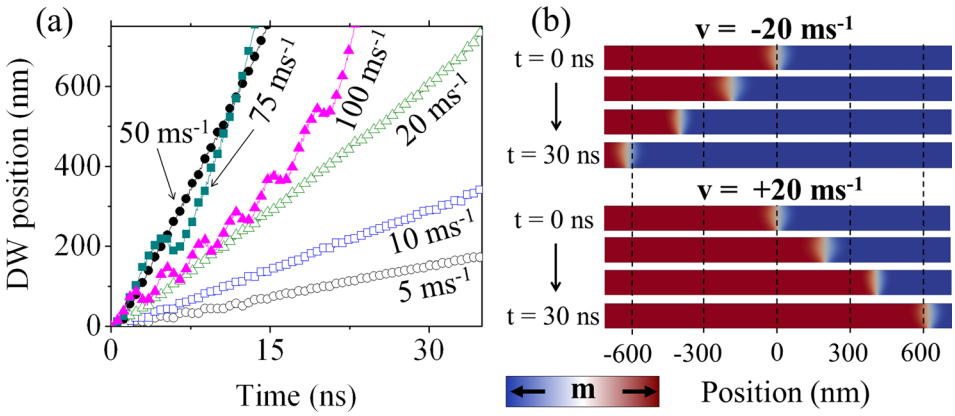

FIG. 4. (a) Dynamics of DWs subjected to standing waves created in moving frames of reference with $v = 5\,\mathrm{ms}^{-1}$ (open circles), $10\,\mathrm{ms}^{-1}$ (open squares), $20\,\mathrm{ms}^{-1}$ (open triangles), $50\,\mathrm{ms}^{-1}$ (closed circles), $75\,\mathrm{ms}^{-1}$ (closed squares), and $100\,\mathrm{ms}^{-1}$ (closed triangles). (b) Simulated dynamics of a domain wall for $v = \pm 20\,\mathrm{ms}^{-1}$. For all of simulations, $A_{SAW} = 30$ MPa, $\lambda = 500$ nm, and $f_{IDT} = 4.23$ GHz.

was applied ($A_{SAW} = 30$ MPa). However, epitaxial $Fe_{81}Ga_{19}$ films have been showed to have saturation magnetostriction constants $\lambda_{100} = 265$ ppm.[27] Performing simulations with these higher values increased the depinning field to $H_x = 25 \pm 5$ Oe, a technologically promising value.

Having demonstrated the feasibility of pinning DWs using SAWs, we turned our attention to inducing DW propagation. Considering the Doppler effect, increasing the frequency of one IDT by Δf, while decreasing the other, creates a standing stress wave in a frame of reference moving with velocity

$$v = \frac{v_{SAW}\Delta f}{f_{IDT}}, \tag{6}$$

where v is the drift velocity of the standing wave relative to the substrate. Hence, by applying frequency shifts to the IDTs, it was expected to be possible to "surf" DWs along the nanowires on the SW's antinodes. For the simulated system, a frequency shift $\Delta f = 2$ MHz was equivalent to a velocity $v = 1\,\mathrm{ms}^{-1}$.

In Fig. 4(a), we present plots of DW position against time for $v = 5\,\mathrm{ms}^{-1}$–$100\,\mathrm{ms}^{-1}$ and $A_{SAW} = 30$ MPa. The DWs were initialised in the centre of the nanowire as in Fig. 1. For $v \leq 50\,\mathrm{ms}^{-1}$, the DWs propagated linearly at velocities equal to v. This indicated that the DWs remained localised at the antinodes during propagation. For $v > 50\,\mathrm{ms}^{-1}$, the DWs exhibited short periods of retrograde motion, and their net velocity began to decrease with increasing v. For example, in Fig. 4(a), the drift velocity of the DWs for $v = 75\,\mathrm{ms}^{-1}$ was $\sim 50\,\mathrm{ms}^{-1}$, while for $v = 100\,\mathrm{ms}^{-1}$ it dropped to $\sim 30\,\mathrm{ms}^{-1}$. This indicates that for $v > 50\,\mathrm{ms}^{-1}$ the DWs were no longer able to move fast enough to travel coherently with the antinodes, and thus their motion became more complex as they interacted with different parts of the SW. The apparent "speed limit" of the DWs corresponded closely to the $50\,\mathrm{ms}^{-1}$ velocity of localisation estimated from Fig. 2(a). DW motion was equivalent for both positive and negative v, as shown in Fig. 4(b), which illustrates DW dynamics for $v = \pm 20\,\mathrm{ms}^{-1}$. We note that the maximum obtainable velocity of $v = 50\,\mathrm{ms}^{-1}$ would require detuning the IDTs by $\Delta f = 100$ MHz, potentially putting them out of resonance. In such a scenario continuously modulating the phases of the transducers would offer an alternative approach to creating a propagating SW.

To probe the feasibility of moving multiple DWs synchronously, we initialised an $l = 4\,\mu$m nanowire in a tri-domain state, with two DWs positioned ± 500 nm from the centre of the nanowire (Fig. 5). Both DWs had magnetisation orientated along $+y$, and thus they had opposite chiralities. We then moved the $1\,\mu$m-long "databit" back and forth $\pm 1\,\mu$m by applying SWs with $v = \pm 20\,\mathrm{ms}^{-1}$.

Fig. 5 demonstrates the transport of the DWs. White dots indicate the locations of the SW antinodes, with additional black dots indicating those at which the DWs were initially localised. The DWs moved synchronously throughout the propagation sequence, thus maintaining the "databit" they delineated. During propagation, the DWs lagged slightly behind the antinodes, to maintain themselves at a position in the SW wave where σ'_{xx} was large enough to sustain their velocity. This led to both DWs moving to follow the antinode directly to the left of that at which they were initially localised during the final part of the sequence. We note that despite having opposite chiralities the DWs appeared to behave equivalently, suggesting that the SAW-DW interactions were chirality independent.

To demonstrate the feasibility of creating SAWs with A_{SAW} of the orders of magnitude considered in this paper,

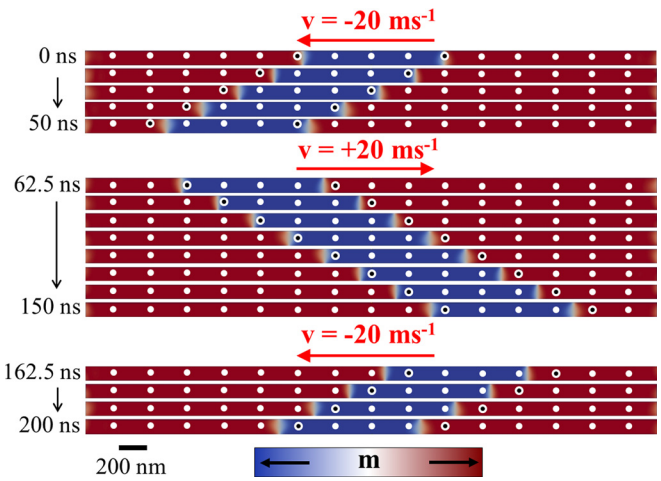

FIG. 5. Synchronous motion of two DWs subjected to standing waves created in moving frames of reference with $v = \pm 20\,\mathrm{ms}^{-1}$. The white dots indicate the positions of the standing wave's antinodes, with additional black dots indicating the antinodes at which the DWs were initially located. $A_{SAW} = 30$ MPa, $\lambda = 500$ nm, and $f_{IDT} = 4.23$ GHz.

we used finite-difference analysis to calculate the stress/strain profile of a SAW induced along the [100] axis of a lithium niobate crystal by an IDT with $s_{IDT} = 125$ nm IDT.[28] The calculations indicated that the profiles of the induced SAWs would deviate from those of an ideal Rayleigh wave, however as DW motion was primarily driven by σ_{xx} we focused on the magnitude of this stress component. For an alternating voltage of ± 1 V applied to the IDT fingers, our calculations predicted a σ_{xx} amplitude equivalent to $A_{SAW} \sim 3$ GPa in the FeGaB layer. Thus, approximately ± 10 V would be required to induce stresses equivalent to the maximum used in our simulations, corresponding to electric fields ~ 160 MVm^{-1} for the chosen value of s_{IDT}. While this is a high value, previous experimental studies have subjected IDTs to high frequency fields of similar magnitude without damage.[29] Furthermore, IDTs can be excited efficiently at their third harmonic, allowing s_{IDT} to be increased, while maintaining the desired SAW wavelength. In combination with utilising more strongly piezoelectric crystal axes, for example, the Y-cut 128° axis, where piezoelectric constants are 3–4 times as large as for the [100] direction,[30] it should be possible to reduce the electric fields imposed on the substrates by an order of magnitude from those calculated above, thus allowing substantial headroom for increasing the strengths of SAW-DW interactions.

In conclusion, we have demonstrated the feasibility of devices where DWs are remotely manipulated using electrically induced SAWs. We have shown that DWs become attracted to, and pinned at, the antinodes of standing stress/strain waves, and used a simple 1D semi-analytical model to explain this in terms of a ratcheted motion towards positions where stress gradients are minimised. We have also demonstrated how multiple DWs can be synchronously propagated at velocities up to 50 ms^{-1} by shifting the frequency of the SAWs.

Our proposed approach has a number of attractive features. First, in materials such as lithium niobate, SAWs can propagate distances $\sim$cm with little power loss.[31] Potentially, this would allow very large numbers of DWs/devices to be controlled by a single transducer pair, making the approach attractive from the perspective of power efficiency. Second, in our approach, DWs are confined to pinning sites during their motion. This could potentially allow DWs motion to be controlled more precisely than in field- and current-induced motion. Finally, in the devices, we propose DW pinning sites are created remotely from the IDTs. Thus, these devices should be simpler to fabricate than previously proposed multi-ferroic devices, where pairs of electric contacts are required for each pinning site.[14] Further investigations will be required to optimise device designs such that both they possess these exciting properties and also allow DWs to be manipulated at speeds that are competitive with conventional approaches.[8–13]

This work was funded by the Engineering and Physical Sciences Research Council (Grant No. EP/J002275/1).

[1]G. Hrkac, J. Dean, and D. A. Allwood, Philos. Trans. R. Soc., A **369**, 3214 (2011).
[2]S. S. P. Parkin, M. Hayashi, and L. Thomas, Science **320**, 190–194 (2008).
[3]G. S. D. Beach, C. Nistor, C. Knutson, M. Tsoi, and J. L. Erskine, Nat. Mater. **4**, 741 (2005).
[4]M. T. Bryan, T. Schrefl, and D. A. Allwood, Appl. Phys. Lett. **91**, 142502 (2007).
[5]A. Himeno, S. Kasai, and T. Ono, Appl. Phys. Lett. **87**, 243108 (2005).
[6]C.-Y. You, Appl. Phys. Lett. **92**, 152507 (2008).
[7]J.-S. Kim, M.-A. Mawass, A. Bisig, B. Krüger, R. Reeve, T. Schulz, F. Büttner, J. Yoon, C.-Y. You, M. Weigand, H. Stoll, G. Schütz, H. J. M. Swagten, B. Koopmans, S. Eisebitt, and M. Kläui, Nat. Commun. **5**, 3429 (2014).
[8]M. Hayashi, L. Thomas, C. Rettner, R. Moriya, Y. B. Bazaliy, and S. S. P. Parkin, Phys. Rev. Lett. **98**, 037204 (2007).
[9]G. Meier, M. Bolte, R. Eiselt, B. Krüger, D.-H. Kim, and P. Fischer, Phys. Rev. Lett. **98**, 187202 (2007).
[10]I. M. Miron, T. Moore, H. Szambo, L. D. Buda-Prejbeanu, S. Auffret, B. Rodmacq, S. Pizzini, J. Vogel, M. Bonfim, A. Schuhl, and G. Gaudin, Nat. Mater. **10**, 423 (2011).
[11]S. Emori, U. Bauer, S.-M. Ahn, E. Martinez, and G. S. D. Beach, Nat. Mater. **12**, 611 (2013).
[12]K.-S. Ryu, L. Thomas, S.-H. Yang, and S. S. P. Parkin, Nat. Nanotechnol. **8**, 527 (2013).
[13]S.-H. Yang, K.-S. Yang, and S. S. P. Parkin, Nat. Nanotechnol. **10**, 221 (2015).
[14]J. Dean, M. T. Bryan, T. Schrefl, and D. A. Allwood, J. Appl. Phys. **109**, 023915 (2011).
[15]C. D. Wood, J. E. Cunningham, R. O'Rorke, C. Walti, E. H. Linfield, A. G. Davies, and S. D. Evans, Appl. Phys. Lett. **94**, 054101 (2009).
[16]J. Cunningham, V. I. Talyanskii, J. Shilton, M. Pepper, M. Y. Simmons, and D. A. Ritchie, Phys. Rev. B **60**, 4850 (1999).
[17]S. Davis, A. Baruth, and S. Adenwalla, Appl. Phys. Lett. **97**, 232507 (2010).
[18]M. Weiler, H. Huebl, F. S. Goerg, F. D. Czeschka, R. Gross, and S. T. B. Gownnenwein, Phys. Rev. Lett. **108**, 176601 (2012).
[19]L. Thevenard, C. Gourdon, J. Y. Prieur, H. J. von Bardeleben, S. Vincent, L. Becerra, L. Largeau, and J.-Y. Duquesne, Phys. Rev. B **90**, 094401 (2014).
[20]W. Li, B. Buford, A. Jander, and P. Dhagat, J. Appl. Phys. **115**, 17E307 (2014).
[21]M. T. Bryan, J. Dean, and D. A. Allwood, Phys. Rev. B **85**, 144411 (2012).
[22]J. Lou, R. E. Insignares, Z. Cai, K. S. Ziemer, M. Lui, and N. X. Sun, Appl. Phys. Lett. **91**, 182504 (2007).
[23]J. L. Rose, *Ultrasonic Waves in Solid Media* (Cambridge University Press, 2004), ISBN: 9780521548892.
[24]J. Dean, M. T. Bryan, G. Hrkac, A. Goncharov, C. L. Freeman, M. A. Bashir, T. Schrefl, and D. A. Allwood, J. Appl. Phys. **108**, 073903 (2010).
[25]R. D. McMichael and M. J. Donahue, IEEE Trans. Magn. **33**, 4167 (1997).
[26]D. G. Porter and M. J. Donahue, J. Appl. Phys. **95**, 6729 (2004).
[27]D. E. Parkes, L. R. Shelford, P. Wadley, V. Holy, M. Wang, A. T. Hindmarch, G. van der Laan, R. P. Campion, K. W. Edmonds, S. A. Cavill, and A. W. Rushforth, Sci. Rep. **3**, 2220 (2013).
[28]J. D. Cooper, Z. Ikonić, J. E. Cunningham, P. Harrison, M. Salih, A. G. Davies, and E. H. Linfield, in *International Conference on Advanced Optoelectronics and Lasers (CAOL)* (2013), p. 22.
[29]F. S. Hickernell, P. L. Clar, and I. R. Cook, in *Proceedings of the 1972 Ultrasonics Symposium* (1972), p. 388.
[30]*Properties of Lithium Niobate*, edited by K. K. Wong (Institution of Engineering and Technology, 2002).
[31]C. K. Campbell, Proc. IEEE **77**, 1453 (1989).